

***n*-alkanes on Pt(111) and on C(0001)/Pt(111): Chain length dependence of kinetic desorption parameters**

Steven L. Tait^{a)}*Department of Physics, University of Washington, Seattle, Washington 98195-1700*

Zdenek Dohnálek

Chemical and Materials Science Division, Fundamental Sciences Directorate, Pacific Northwest National Laboratory, Richland, Washington 99352

Charles T. Campbell

*Department of Chemistry, University of Washington, Seattle, Washington 98195-1700*Bruce D. Kay^{b)}*Chemical and Materials Science Division, Fundamental Sciences Directorate, Pacific Northwest National Laboratory, Richland, Washington 99352*

(Received 29 August 2006; accepted 27 October 2006; published online 20 December 2006)

We have measured the desorption of seven small *n*-alkanes (C_NH_{2N+2} , $N=1-4,6,8,10$) from the Pt(111) and C(0001) surfaces by temperature programmed desorption. We compare these results to our recent study of the desorption kinetics of these molecules on MgO(100) [J. Chem. Phys. **122**, 164708 (2005)]. There we showed an increase in the desorption preexponential factor by several orders of magnitude with increasing *n*-alkane chain length and a linear desorption energy scaling with a small *y*-intercept value. We suggest that the significant increase in desorption prefactor with chain length is not particular to the MgO(100) surface, but is a general effect for desorption of the small *n*-alkanes. This argument is supported by statistical mechanical arguments for the increase in the entropy gain of the molecules upon desorption. In this work, we demonstrate that this hypothesis holds true on both a metal surface and a graphite surface. We observe an increase in prefactor by five orders of magnitude over the range of *n*-alkane chain lengths studied here. On each surface, the desorption energies of the *n*-alkanes are found to increase linearly with the molecule chain length and have a small *y*-intercept value. Prior results of other groups have yielded a linear desorption energy scaling with chain length that has unphysically large *y*-intercept values. We demonstrate that by allowing the prefactor to increase according to our model, a reanalysis of their data resolves this *y*-intercept problem to some degree. © 2006 American Institute of Physics.

[DOI: [10.1063/1.2400235](https://doi.org/10.1063/1.2400235)]

I. INTRODUCTION

Understanding the dependence of desorption energy on *n*-alkane chain length is a topic of current interest for a wide range of industrial applications (e.g., catalysis, chemical sensing, and geochemistry), as well as for understanding the basic physics behind the chain length scaling of the desorption energy and desorption rate preexponential factor. We have reported recently a linear increase in desorption energy along with a rise of several orders of magnitude in preexponential factor for *n*-alkane desorption from MgO(100).¹ We demonstrated in that work that the large rise in desorption prefactor with chain length should be expected based on a simple statistical mechanical model. We suggest that this strong rise in prefactor with chain length is a general (i.e., substrate independent) effect for the small *n*-alkanes. In this work, we confirm this hypothesis for *n*-alkane desorption from Pt(111) and from a graphite film.

The desorption of small *n*-alkane molecules has been studied on many metal surfaces, such as Ag(110),² Au(111),³ Cu(111),⁴ Cu(100),^{5,6} Pt(111),^{4,7-12} and Ru(001),¹³ as well as on Al₂O₃(0001),¹⁴ MgO(100),¹ C(0001),¹⁵⁻¹⁷ and Si(111) (Ref. 18) surfaces. Some of these studies have explored the dependence of the desorption kinetics on *n*-alkane chain length. For short *n*-alkane molecules (C_NH_{2N+2} , $N < 12$), the desorption energy is typically observed to scale linearly with *n*-alkane chain length, *N*, consistent with a simple picture of the desorption energy increasing proportionally to the number of C chain segments interacting with the substrate. Although there is a linear relationship between the desorption energy and chain length (nearly constant incremental increase in desorption energy per unit increase in chain length), this linear function is observed to have a nonzero offset when extrapolated to zero chain length ($N=0$) in many of the above-cited studies. That is, a linear regression of the desorption energy versus chain length (E_d vs N) data yields a good fit to the experimental results, but the resulting fit line has a nonzero *y*-intercept value. Such a *y*-intercept offset is inconsistent with the interpretation of the energy simply increasing

^{a)}Present address: Max Planck Institute for Solid State Research, Heisenbergstrasse 1, 70195 Stuttgart, Germany.

^{b)}Author to whom correspondence should be addressed. Fax: (509) 376-6066. Electronic mail: bruce.kay@pnl.gov

proportionally to the number of C segments interacting with the substrate. It had been suggested that part of this y -intercept offset could be due to differences in the adsorption strength of the $-\text{CH}_3$ end-group segments compared to the $-\text{CH}_2-$ segments in the interior of the molecule. However, this explanation is generally dismissed since the magnitude of the previously reported y -intercept values would require that the $-\text{CH}_3$ interactions be several times greater than the $-\text{CH}_2-$ interactions.⁷ There has also been a study to show that in cyclic alkanes, where no “end groups” exist, this y -intercept problem persists.⁴

Molecular dynamics simulations of small n -alkane ($N=1-12$) desorption from Au(111) (Ref. 19) and from C(0001) (Ref. 20) have helped to resolve the y -intercept problem. In both studies an increase in desorption prefactor of several orders of magnitude with increasing chain length in the range $N=1-12$ was predicted [Au(111): $10^{12.2} \text{ s}^{-1}$ for CH_4 to $10^{16.4} \text{ s}^{-1}$ for $\text{C}_{12}\text{H}_{26}$, C(0001): $10^{15.1} \text{ s}^{-1}$ for C_5H_{12} to $10^{17.7} \text{ s}^{-1}$ for $\text{C}_{12}\text{H}_{26}$] in the limit of low molecule coverage. This increase in prefactor is attributed to a growing difference between the entropy of the molecule in the adsorbed state and the entropy of the molecule in the gas-phase-like transition state with increasing chain length.¹⁹ It was also shown that the desorption energies increased linearly with chain length, but that when the prefactor is assumed to be simply 10^{13} s^{-1} for all n -alkanes, the desorption energy scales in a less than linear way with chain length.¹⁹

In the case of the desorption of seven small n -alkanes in the range $N=1-10$ from the MgO(100) surface,¹ we also found the desorption energy to increase linearly with n -alkane chain length. We utilized a quantitative mathematical analysis method which allowed us to extract both a chain-length-dependent desorption prefactor and a coverage-dependent desorption energy from the temperature programmed desorption (TPD) experimental data.²¹ That is, rather than assuming a single value for the prefactor for all n -alkanes, we obtained a prefactor result for each n -alkane from the experimental data. These results were sufficiently accurate and robust to simulate TPD spectra over a wide range of initial coverages and temperature ramp rates that matched the experimental data very well. The problem of a large nonzero offset in the desorption energy versus chain length plot, which has been reported in other studies on different substrates, would have shown up in our data as well if we had assumed a prefactor that was constant with n -alkane chain length in our data analysis. However, when the prefactor was allowed to vary with chain length in the analysis, we found that the linear relationship between the n -alkane desorption energy and chain length had a y -intercept offset that is small compared to the incremental increase in energy with unit increase in chain length (i.e., offset from zero energy when linear regression extrapolated to $N=0$ was less than slope of linear regression).

A notable finding from our previous study was that the desorption prefactors, typically assumed to be about 10^{13} s^{-1} for small molecule desorption, increased by six orders of magnitude over the short range of molecule chain lengths studied. We demonstrated there that such a significant increase in prefactor with chain length can be accounted for by

considering the rotational and translational entropy gains of the molecules as they desorb from the adsorbed state [essentially confined to the two-dimensional (2D) surface plane] to the transition state [freely rotating in three dimensions (3D) and translating in 2D]. These arguments are discussed in greater detail in Sec. III below. This interpretation relies on the fundamental principles of statistical mechanics and does not rely on the specific attributes of the adsorbate interaction with the substrate. An increase in desorption prefactor with increasing molecule size for rigid molecules should therefore be a general effect. The precise values of the prefactors will of course depend on the entropy of the molecule in the adsorbed state, but for this set of small n -alkane molecules, this statistical model shows that there must be a significant increase in the desorption prefactor with chain length for desorption from any substrate. We have demonstrated this previously for desorption from an oxide surface¹ and here will show that this argument holds for desorption of the small n -alkanes from a metal (Pt) surface as well as a graphite surface. Accounting for this increase in prefactor in our results has relieved much of the nonzero y -intercept problem in the linear regression to our desorption energy versus chain length data. We suspect that accounting for this effect would remove this issue from the works of other groups as well and here we demonstrate for a few cases that indeed it does.

In this work, we measure the desorption kinetics of a series of small n -alkane molecules ($\text{C}_N\text{H}_{2N+2}$, $N=1-4,6,8,10$) from Pt(111) and graphitic C(0001). We apply the inversion-optimization analysis method discussed previously to extract kinetic parameters,²¹ and discuss the dependence of the desorption prefactor and energy on n -alkane chain length. We will make a direct comparison of our results to the results of four previous works, including studies by three groups of n -alkane desorption from the Pt(111) surface⁷⁻¹¹ and a study by Paserba and Gellman on graphite.¹⁵

The first of these studies on Pt(111) was the work of Salmeron and Somorjai⁸ to study the desorption of n -butane and n -pentane by TPD. They obtained prefactor results of $10^{11.0}$ and $10^{11.6} \text{ s}^{-1}$, respectively, nearly four orders of magnitude lower than our prefactor result for n -butane. We believe that this discrepancy may be due, in part, to the high heating rate (10 K/s) used in their work, which leads to peak broadening in their TPD data.⁸ They attempt to minimize the effect of the peak broadening on their results for the desorption-kinetics parameters by making fits to the first half of the desorption peaks (from half maximum on the low-temperature side to peak maximum). It has been demonstrated, however, that at high ramp rates, the peak not only broadens, but the leading edge will shift and the peak shape can become distorted.²¹

Bishop *et al.* reported on desorption of $N=6-10$ from Pt(111).⁷ From a simple Redhead analysis they obtained desorption energies based on an assumed prefactor of 10^{13} s^{-1} . They noted that the nonzero intercept in the plot of E_d vs N is much too large to be accounted for by a difference in methane and methylene segment adsorption. According to their estimate, their observation would require that the adsorption strength of a $-\text{CH}_3$ segment be six times greater

than for a $-\text{CH}_2-$ segment. They commented that to account for the decrease in per-C segment E_d with chain length there must be a large increase in prefactor with chain length, but their ramp rate experiments yield prefactors of approximately 10^{13} s^{-1} and so they concluded that the problem with their energy values is due to the simplicity of the first-order rate law (Redhead equation) used in the data analysis. They commented that part of the problem may be due to interadsorbate interactions which are not accounted for by the simple rate law. In our analysis we have used a coverage-dependent desorption energy to allow for these interactions.

Madix and co-workers have made several studies of *n*-alkane adsorption or trapping on transition metal surfaces. In several of these articles, they also commented on the desorption kinetics measured by TPD for methane, ethane, propane, and *n*-butane from Pt(111) (Refs. 9–11) and reported desorption energies, but not prefactors.⁹ Those are the desorption energies that we make comparison to later in this paper. They also presented desorption energies at low coverages of each molecule, along with prefactors on the order of 10^{14} – 10^{16} s^{-1} , but not showing a trend with increasing chain length.

Paserba and Gellman studied the desorption of 21 *n*-alkanes in the range $N=5$ – 60 from graphite.¹⁵ These results show a nonlinear dependence of desorption energy on chain length due to partial detachment conformational entropy, which is not expected to play a significant role for the small *n*-alkanes ($N < 12$).^{15,16} For a subset of nine *n*-alkanes ($N=7, 12, 24, 26, 28, 32, 36, 40,$ and 44), they obtained prefactor results from a heating ramp rate variation and concluded that the prefactor is independent of chain length over this molecule range, with an average value of $10^{19.6} \text{ s}^{-1}$. However, only one of those molecules for which the prefactor was actually measured ($N=7$) lies within the range of molecules in our study and it has the smallest prefactor result of $10^{18.7} \text{ s}^{-1}$ of the molecules they studied. The next largest molecule for which the prefactor was measured was *n*-dodecane ($N=12$) with a prefactor of $10^{20.3} \text{ s}^{-1}$. In our study of desorption from graphite, we observed that the prefactors of the larger *n*-alkanes ($N=6, 8,$ and 10) are not increasing strongly with chain length compared to the sharp increase for the smaller molecules ($N=1$ – 6), i.e., the prefactor increase seems to be “rounding off” as N approaches 10. The conclusion drawn by Paserba and Gellman of the prefactor having a little variation over a wide chain length range ($N=7$ – 44) is not inconsistent with our results on graphite which show an increase in prefactor up to $N=6$ (our prefactor result for *n*-hexane was $10^{16.5} \text{ s}^{-1}$).

In this paper, we present the results of a detailed study of the desorption kinetics of seven small *n*-alkanes from the Pt(111) and C(0001)/Pt(111) surfaces using TPD. The experimental apparatus used in this work allows for sample cooling to temperatures below 25 K. This has allowed us to extend our study of the chain length scaling of the desorption kinetics of the *n*-alkanes to the smallest *n*-alkanes, which have not been accessible to many previous works, including three of those mentioned above. The data analysis in this work follows the inversion-optimization analysis method presented previously.²¹ We will apply that analysis method to

these *n*-alkane desorption measurements from Pt(111) and C(0001)/Pt(111) and determine the kinetic parameters (desorption energies and prefactors) of *n*-alkane desorption from these surfaces. The results will be compared to those for MgO(100), which were presented previously.¹

II. EXPERIMENT

The apparatus used for these experiments was a molecular beam/surface scattering system at the Pacific Northwest National Laboratory, which has been described in detail elsewhere.²² The TPD experiments in this work were conducted under ultrahigh vacuum conditions, with base pressure $\sim 1 \times 10^{-10}$ Torr.

The Pt(111) single crystal substrate was cleaned using standard procedures consisting of several cycles of sputtering with 1.5 keV Ne^+ ions and annealing at 1200 K in 10^{-6} Torr O_2 and subsequently in UHV. The Pt(111) surface was found to be highly ordered as evidenced by a very sharp low energy electron diffraction (LEED) pattern and small population of defect states in N_2 and CH_4 TPD spectra.

The graphite surface was a highly-ordered, one monolayer thick graphitic carbon film, prepared by dissociation of *n*-decane on the Pt(111) substrate, similar to the procedure developed in prior studies.^{23–26} The Pt(111) substrate was held at 1200 K while a molecular beam of *n*-decane was impinged on the surface. This graphite overlayer was shown previously to have a lattice spacing within 0.5% of the bulk graphite lattice spacing.²³ We refer to that surface herein as C(0001)/Pt(111). We consistently found the graphitic surface prepared in this manner to have a low defect density by TPD measurements (see below).

The MgO(100) surface was a high quality film produced by vapor deposition of Mg from a directional source in a background of 1×10^{-6} Torr O_2 onto a Mo(100) substrate held at 600 K. The sample was then annealed at 1000 K in the O_2 background. Preparation of these films has been described previously²¹ and has been shown to result in a high quality oxide surface with defect densities comparable to single crystal MgO.²²

The adsorbate molecules in this work were straight chain *n*-alkanes: methane, ethane, propane, *n*-butane, *n*-hexane, *n*-octane, and *n*-decane ($\text{C}_N\text{H}_{2N+2}$, $N=1$ – $4, 6, 8,$ and 10). Liquid phase molecules ($N=6, 8, 10$) were purified by several freeze-pump-thaw cycles before introduction to the molecular beam system. During deposition, the beam nozzle was held at room temperature and the sample was held at a temperature well below the multilayer desorption temperature for that molecule. A quadrupole mass spectrometer (QMS) in a line-of-sight position measured the reflected flux of the molecular beam.

Temperature programmed desorption (TPD) measurements were made by ramping the temperature of the sample at a constant rate (0.6 K/s) and measuring the desorption of the molecule by QMS in the same line-of-sight position as during deposition. TPD experiments were made at many initial coverages for each molecule on each of the substrates. We also made TPD measurements at several other heating rates for each molecule which are not shown here, but are consis-

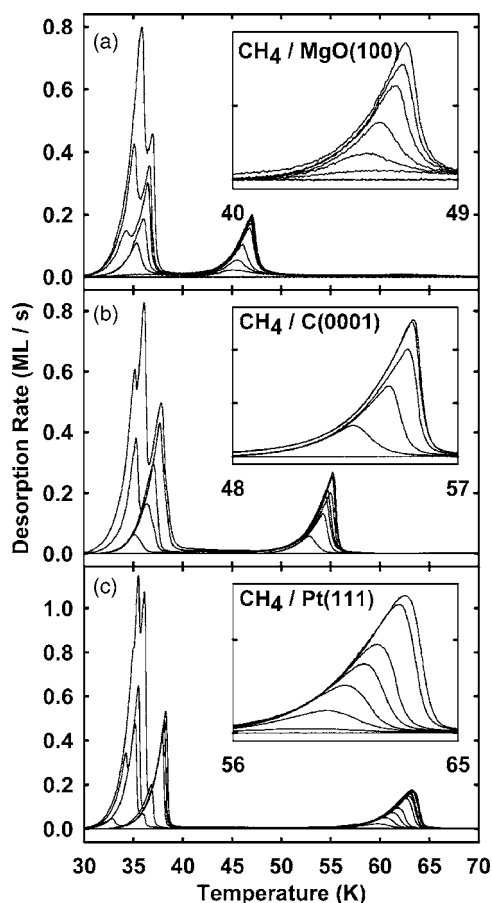


FIG. 1. Temperature programmed desorption spectra of methane from (a) MgO(100), (b) C(0001)/Pt(111), and (c) Pt(111). In each frame, several TPD spectra are plotted, each corresponding to a different initial coverage of CH₄. The high-temperature peak is desorption of the first monolayer of methane from the surface. The other peaks correspond to desorption of the second, third, and higher layers of methane (in order of decreasing peak temperature). The inset in each frame shows detail of the TPD peak for desorption of the first monolayer of methane on the surface. The multilayer desorption occurs at the same temperature on each substrate, but the second and first layer peaks are at different temperatures on each substrate in the order MgO < C < Pt. The heating ramp rate in the TPD experiments in this as well as the other figures was 0.6 K/s. Results on MgO (a) are reproduced here from Ref. 1.

tent with the present TPD results. Rather than conducting an analysis here based on experiments using a wide range of heating rates, as we did in our related study of these alkanes on MgO(100),¹ we have analyzed our data here using only a single, mid-range heating rate and the inversion-optimization method described in Ref. 21. We have shown elsewhere that this simpler approach gives kinetic parameters that agree very well with those obtained by fitting experiments over a wide range of heating rates.¹

III. RESULTS AND DISCUSSION

A. Temperature programmed desorption results

In Fig. 1, we have plotted desorption spectra for methane from (a) MgO(100), (b) C(0001)/Pt(111), and (c) Pt(111). For each substrate, several representative spectra are plotted, corresponding to different initial coverages of methane. In each case there is a peak for desorption of the first monolayer of CH₄ from the surface (highest temperature peak, shown in

detail in each inset) which is well resolved from the desorption peaks of the higher layers. This monolayer desorption peak is the one that is used in our detailed kinetic analysis below. We define a full monolayer coverage of molecules on the surface ($\theta=1.0$ ML) by the saturation of this peak (thus the absolute number of molecules per unit area in 1 ML decreases with increasing N). In each of these spectra it is also possible to resolve the desorption peak of the second layer of molecules from the peak corresponding to the third and higher layers (multilayer peak). In the cases of C and Pt substrates the third layer desorption peak is also resolved from the multilayer peak (lowest temperature peak). We see that the desorption temperature of the monolayer of methane increases on the surfaces in the order MgO < C < Pt and that the second layer desorption peak follows the same trend. We will discuss these spectra in greater detail below.

TPD spectra are shown in Fig. 2 for desorption of (a) ethane, (b) propane, (c) *n*-butane, and (d) *n*-hexane from Pt(111). For each molecule, seven representative spectra are plotted corresponding to different initial coverages in the range of 0–2 ML. We recorded similar data at several other initial coverages for each molecule, which are not shown here for clarity of presentation, but which were used in the following analysis. Note that the scales of both the temperature (horizontal) axis and the desorption rate (vertical) axis are different for each panel in Fig. 2 (scaling factors for the vertical axis are given in the caption). In each set of these TPD spectra, we see two distinct peaks corresponding to desorption of the second layer of the molecule (low temperature) and desorption of its first monolayer (higher temperature).

For methane and ethane desorption from Pt(111) [Figs. 1(c) and 2(a), respectively], we see an increase in the monolayer desorption peak temperature of ~ 3 –4 K with increasing initial coverage in the range of 0–1 ML. The desorption appears to be nearly zero order in nature, due to the fact that desorption occurs through a 2D adsorbate gas which is in a quasiequilibrium with condensed 2D adsorbate islands on the surface.²⁷ The evolution of the monolayer TPD line shape from zero-order-like to first-order-like with increasing chain length is most likely related to the breakdown of the quasiequilibrium in the two-phase coexistence between 2D gas and 2D condensed adsorbate phases in the monolayer, due to reduced adsorbate mobility. It seems that the smaller molecules are able to migrate more easily on the surface than the larger molecules, and thus they are not kinetically prevented from moving into the most stable structure and maintaining this quasiequilibrium, hence their desorption peaks are more zero-order-like.

The *n*-butane monolayer desorption peak position is unchanged for the four smallest initial coverages, but at higher initial coverages, the leading edge of the peak shifts significantly to lower temperature [Fig. 2(c)]. It has been observed previously that the *n*-butane fills in an ordered monolayer up to a coverage of about 0.6 ML on Pt(111) (0.2 *n*-butane molecules/Pt surface atom), then from 0.6 to 1.0 ML the *n*-butane molecules tilt away from the surface slightly.¹⁰ The effect of *n*-butane tilting away from the Pt(111) surface with increasing coverage was also predicted in molecular dynam-

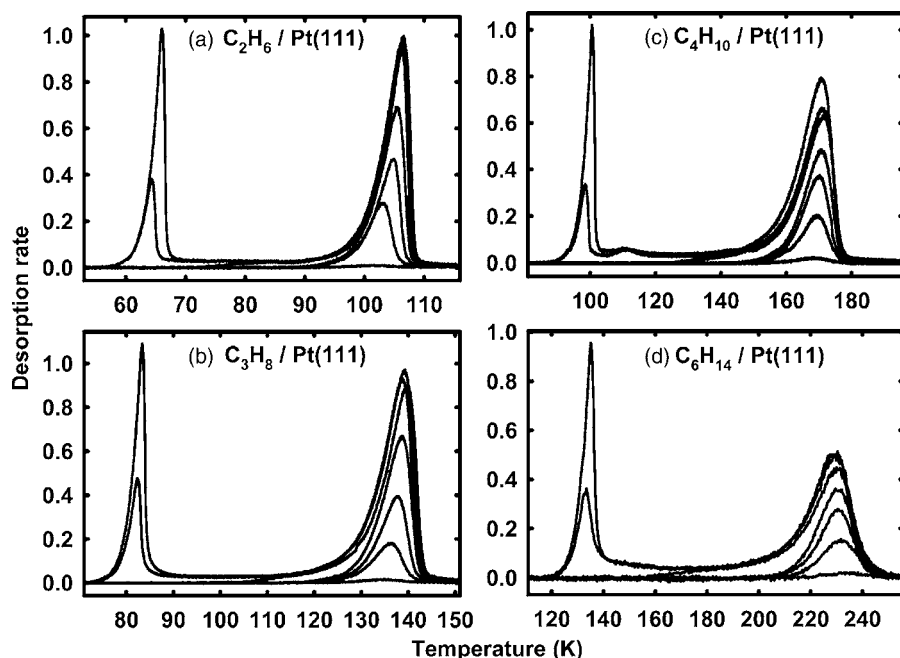


FIG. 2. Summary of TPD experiments on Pt(111) for (a) ethane, (b) propane, (c) *n*-butane, and (d) *n*-hexane. In each frame, seven desorption spectra are plotted corresponding to different initial coverages in the range of 0–2 ML. Desorptions of the first and second layers of molecules are clearly resolved in each frame as two distinct peaks. For the larger molecules there is a nonzero desorption rate (plateau regions) between the peaks, corresponding to molecule compression in the first layer, as discussed in the text. Note that the temperature scale is different in each frame, as labeled. The desorption rate scales have been normalized and should be multiplied by the following constants in order to obtain the desorption rate in units of ML/s: (a) 0.05, (b) 0.05, (c) 0.025, and (d) 0.004.

ics simulations by Raut *et al.*²⁸ This tilting allows the molecules to pack more closely on the surface, and may account for the abrupt shift in peak shape in our TPD experiment.

The alignment of the high-temperature side of the monolayer desorption peaks of the TPD spectra for *n*-hexane [Fig. 2(d)] is probably indicative of a very slight repulsive interaction between the *n*-hexane molecules even at relatively small ($> \sim 0.2$ ML) submonolayer coverages. The small magnitude of this repulsion is evidenced by the very slight shift (only a few degrees) of the TPD peak to lower temperature with increasing coverage and may be related to a dipole-dipole repulsion on the Pt(111) surface, where large dipole moments of hydrocarbons have been observed previously.²⁹

The separation of the first and second monolayer peaks for the larger molecules [Figs. 2(c) and 2(d)] is not as distinct as for the smaller molecules [Figs. 1(c), 2(a), and 2(b)] (i.e., desorption rate is nonzero between the peaks). For coverages nearing completion of the monolayer, adsorbate compression gives rise to repulsive interactions that manifest themselves as the broad plateau region having a small, but easily detectable desorption rate between the monolayer and second layer TPD peaks.³⁰ Simply stated, as the coverage increases in the plateau region, the monolayer chemical potential increases continually with increasing coverage until it attains the chemical potential of the less stable second layer. This same argument also applies to the data in Fig. 3.

The longest two *n*-alkanes that we studied (*n*-octane and *n*-decane) were found to dissociate upon adsorption on Pt(111), even at low substrate temperature (100 and 140 K, respectively). We observed distortion of the *n*-octane spectra which may be due to accumulation of dissociated *n*-octane fragments on the surface after multiple experiments. In a series of *n*-octane experiments where the sequence of *n*-octane exposures (dose time from molecular beam) was randomized we found that the monolayer desorption peak area decreased (consistent with surface contamination by molecule fragments) and shifted to higher temperature. The

shape and position of the monolayer peak were not reproducible unless the Pt surface was sputtered and annealed to clean it after each experiment, indicating that *n*-octane leaves dissociation fragments on the surface. A similar effect, but to a greater degree, was observed for *n*-decane adsorption at Pt(111). Therefore the results for *n*-octane and *n*-decane desorption are omitted from our analysis of the molecular desorption kinetics.

In Fig. 3, we summarize results for *n*-alkane desorption from the graphitic C(0001)/Pt(111) surface. Here we plot results for (a) ethane, (b) propane, (c) *n*-butane, (d) *n*-hexane, (e) *n*-octane, and (f) *n*-decane. In this case, the monolayer desorption peaks for methane, ethane, propane, and *n*-butane [Figs. 1(b) and 3(a)–3(c)] appear nearly zero order in nature. For all seven of the molecules there is a noticeable increase in monolayer desorption peak temperature with increasing initial coverage.

For ethane desorption from C(0001)/Pt(111) [Fig. 3(a)], there is a small peak just to higher temperature from the multilayer peak. This peak is positioned where we would expect to see a second layer peak (close to, but slightly higher than multilayer desorption temperature), but the area under this peak is too small (compared to the monolayer peak area) to account for an entire second layer. We have compared the amount of ethane dosed on this surface in order to saturate the monolayer peak to the dose required to saturate the monolayer peak on Pt(111) and find that these dose amounts are nearly exactly the same. Thus, the small peak at 65 K in the ethane/C(0001)/Pt(111) desorption spectrum is apparently some state intermediate between the monolayer and multilayer. LEED studies of ethane adsorption on graphite surfaces have shown that at low coverages and temperatures the ethane molecules lie parallel to the graphite surface, but as coverage increases above 0.7 ML the molecules reorder on the surface and by 1.0 ML, the ethane molecules are standing with the C–C bond perpendicular to the surface.³¹ It may be that this desorption peak at 65 K is

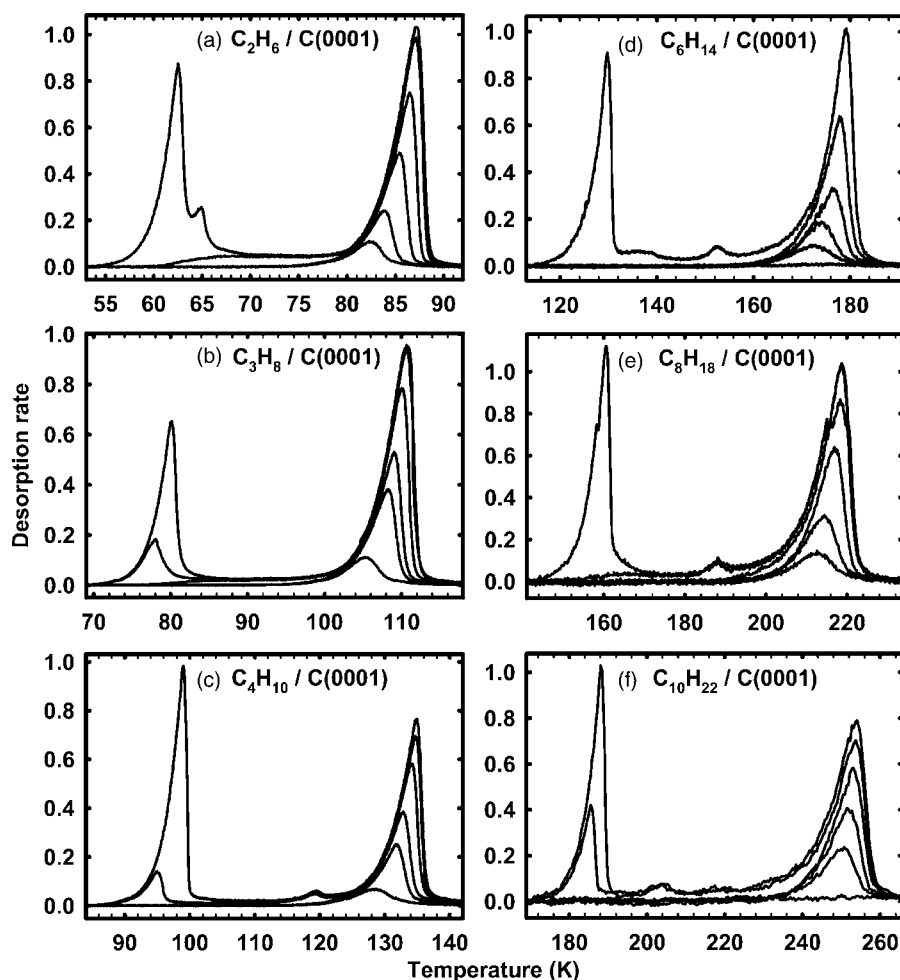


FIG. 3. Summary of temperature programmed desorption (TPD) experiments on C(0001)/Pt(111) for (a) ethane, (b) propane, (c) *n*-butane, (d) *n*-hexane, (e) *n*-octane, and (f) *n*-decane. Seven desorption spectra are plotted in each frame, corresponding to different initial molecule coverages in the range of 0.2 ML. Desorptions of the first and second layers of molecules are seen here as two distinct peaks separated by a region of nonzero desorption energy. A less-noticeable third peak is present between the two major peaks in all but the propane spectra. This may be due to a structural transition of the molecules as discussed in the text. Note that the temperature scale is different in each frame, as labeled. The desorption rate scales have been normalized and should be multiplied by the following constants in order to obtain the desorption rate in units of ML/s: (a) 0.08, (b) 0.10, (c) 0.06, (d) 0.008, (e) 0.0025, and (f) 0.001.

related to the structural transition of ethane molecules from a standing to flat-lying geometry. To our knowledge, this transition has not been observed to occur for ethane on Pt(111). We see similar small peaks in the desorption spectra for *n*-butane, *n*-hexane, *n*-octane, and *n*-decane on C(0001) and for *n*-butane on Pt(111) [Fig. 2(c)].

The region of the TPD spectrum showing the saturated monolayer desorption peak is plotted in Fig. 4 for each of the seven *n*-alkanes on each of the three substrates studied. The trend of higher desorption temperature in the order MgO < C < Pt holds true for all seven molecules. In Fig. 4(b) we have plotted these TPD spectra on a log(temperature) scale to illustrate that the ratio of the desorption temperatures for a given molecule from any two of the substrates is approximately constant for each of these molecules and substrates. We also note that for each substrate the ratio of the desorption peak width to the peak position is approximately constant for the full range of molecules. Since Fig. 4(b) is a log plot only along the temperature axis, the peak area corresponding to 1 ML is not constant as a function of temperature as it is in Fig. 4(a), but decreases with increasing temperature.

B. Inversion-optimization analysis

We have applied the inversion-optimization analysis method described in detail in Ref. 21 to these data. Briefly, a TPD spectrum for an initial coverage greater than 1 ML was

used to calculate desorption energy as a function of coverage by inverting the (first-order) Polanyi-Wigner equation, which expresses the desorption rate, r , as a function of coverage, θ , and temperature, T ,

$$r(\theta, T) = -\frac{d\theta}{dt}(\theta, T) = \nu\theta e^{-E_d(\theta)/k_B T}, \quad (1)$$

where k_B is the Boltzmann constant. Then the resulting energy versus coverage (E_d vs θ) curve, obtained by assuming some (coverage-independent) preexponential factor, ν , is used to simulate TPD for five initial coverage less than 1 ML. The χ^2 error, defined as the sum of the squares of the differences between simulation and experimental data points, was calculated. This was repeated for several assumed values of prefactor until a well defined minimum in χ^2 was found, giving the “best fit” prefactor. In short, the prefactor is treated as a variational parameter to minimize the residual error between the experimental TPD data and simulated TPD spectra, where the simulations are based on a single desorption energy versus coverage function calculated with the prefactor.

The simulated spectra from the best fit prefactors and coverage-dependent energies are plotted for a representative set of *n*-alkanes as solid lines, along with the experimental data as solid points, in Fig. 5 for desorption from Pt(111) and in Fig. 6 for C(0001)/Pt(111). Agreement between simulation and experiment is very good for the best fit prefactor

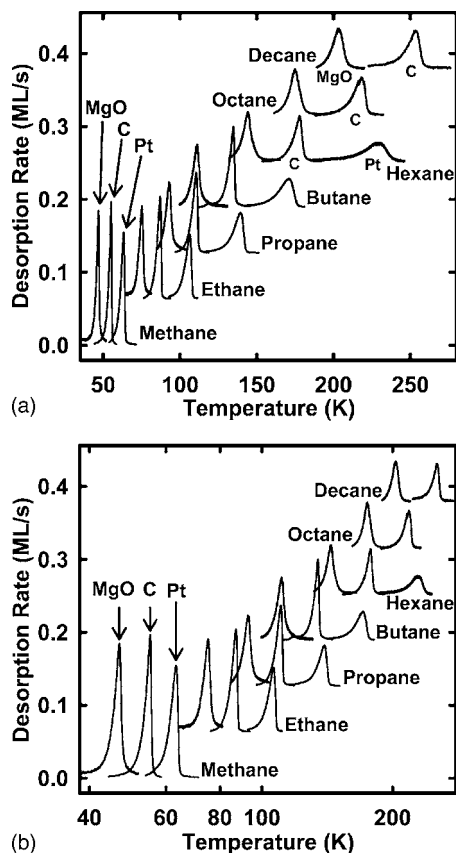


FIG. 4. Summary of TPD data for small *n*-alkanes on MgO(100), C(0001)/Pt(111), and Pt(111). The saturated monolayer desorption peaks are plotted here for each of the seven *n*-alkanes studied on each of the three substrates. They are offset vertically and labeled to indicate desorption from MgO, C/Pt[C], or Pt. In the case of each of the molecules the desorption temperature increases in the order MgO < C < Pt. In (a) we have plotted these vs a linear temperature scale and in (b) they are plotted vs a log temperature scale to emphasize that the ratio of the desorption peak temperatures for any two of the substrates is approximately constant for each molecule.

values for these five initial coverages (approximately 0.2, 0.4, 0.6, 0.8, and 1.0 ML), demonstrating the reliability of our inversion-optimization analysis method over this range of *n*-alkane chain lengths. Fits to the desorption spectra for the other *n*-alkanes are not shown here, but are of the same high quality. The line shapes of the desorption peaks in each case are reproduced very well by the simulation. The coverage dependence of the desorption-kinetics parameters is essential for capturing the subtle deviations in the peak shape from ideal TPD line shapes.

The log of the prefactor which was used to obtain the best fit between the simulation and experiment is listed in Table I and plotted as a function of *n*-alkane chain length in Fig. 7 for each molecule from both the Pt(111) and C(0001)/Pt(111) substrates (represented by triangular and square symbols, respectively). Data points for desorption from MgO(100) are reproduced here (circles in Fig. 7) from Ref. 1 for comparison. We consider a $\pm 10\%$ uncertainty in the log of the prefactor to be an upper limit on the uncertainty in the prefactor due to experimental error.²¹ We represent this uncertainty with an error bar on the two points in Fig. 7 for the methane and *n*-decane desorption from

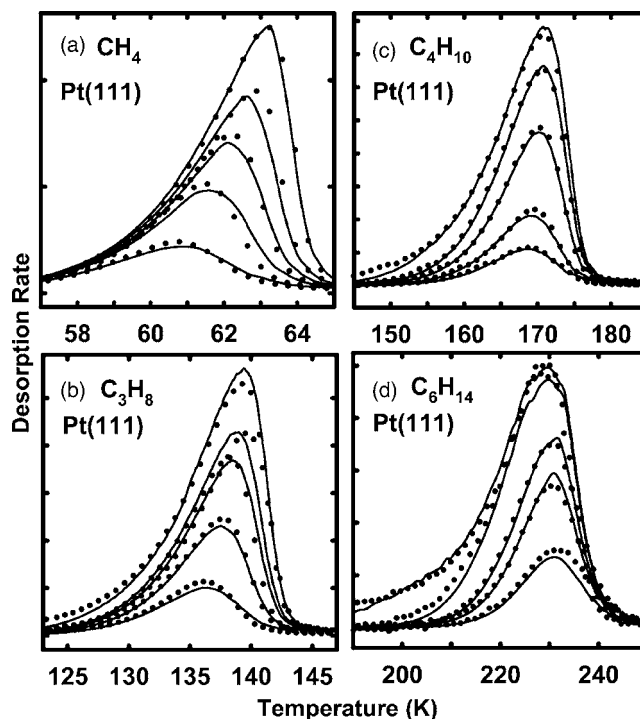


FIG. 5. Comparison of experimental (dot points) and simulated (solid line) TPD data for desorption of (a) methane, (b) propane, (c) *n*-butane, and (d) *n*-hexane from Pt(111). Simulations are based on an assumed value of the prefactor and a coverage-dependent desorption energy calculated from a single TPD spectrum. The prefactor is varied (requiring recalculation of the desorption energy) to optimize the fit of the simulations to experimental data for five initial coverages. Note that the scaling and range of the temperature axis for each frame are different and that the tick marks on the vertical axis each correspond to 0.05 ML/s desorption rate in frame (a) and 0.01 ML/s in frames (b)–(d).

C(0001)/Pt(111), but omit the error bars on the other points for clarity of presentation. The dashed lines in Fig. 7 represent the theoretical limits on the prefactors, as discussed in the next section. We see that the prefactor increases by about five orders of magnitude over the range of molecules studied on both the Pt(111) and the C(0001)/Pt(111) surfaces. The dramatic increase of prefactor with chain length is similar to that observed previously for MgO(100).¹ This large variation highlights the importance of allowing the value of the prefactor to vary with alkane chain length in the TPD analysis.

C. Prefactor limits

Theoretical limits on the prefactor are plotted as dashed lines in Fig. 7. In our discussion of the large observed increase of the desorption prefactor with *n*-alkane chain length from MgO(100),¹ we presented two models based on transition state theory (TST) that set bounds on the possible range of prefactors for small *n*-alkane desorption. We will briefly review those models here in order to evaluate limits on the prefactors for desorption from Pt(111) and C(0001).

The preexponential factor for an elementary process such as molecular desorption can be calculated from the ratio of the partition function of the molecule in the transition state, q^\ddagger , to the partition function of the molecule in the initial state, q_{ads} , using transition state theory,³²

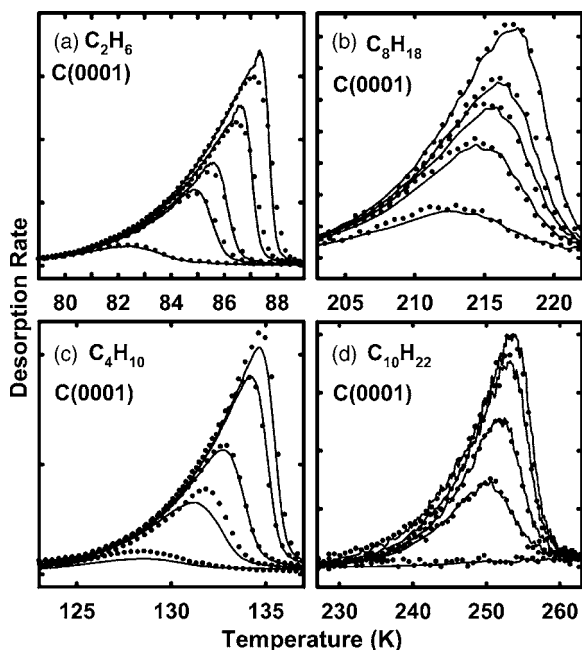


FIG. 6. Comparison of experimental (dot points) and simulated (solid line) TPD data for desorption of (a) ethane, (b) *n*-butane, (c) *n*-octane, and (d) *n*-decane from C(0001)/Pt(111). Simulations are based on an assumed value of the prefactor and a coverage-dependent desorption energy calculated from a single TPD spectrum. The prefactor is varied (requiring recalculation of the desorption energy) to optimize the fit of the simulations to experimental data for five initial coverages. Note that the scaling and range of the temperature axis for each frame are different and that the tick marks on the vertical axis each correspond to 0.05 ML/s desorption rate in frames (a) and (b) and 0.01 ML/s in frames (c) and (d).

$$\nu_{\text{TST}} = \left(\frac{k_B T}{h} \right) \frac{q^\ddagger}{q_{\text{ads}}} \quad (2)$$

Note that the degree of freedom along the reaction coordinate is omitted from the calculation of q^\ddagger . For an adsorption/desorption process with no free energy barrier to adsorption, such as the present case, the transition state is equivalent to the final state of the molecule, namely, its gas phase, without the translational degree of freedom normal to the surface. That is, the molecules have full freedom of rotational motion in 3D and translation motion in 2D at the transition state. The initial state for the desorption process is the adsorbed state of the molecule. Exact calculation of the partition function for this state would require a detailed knowledge of the

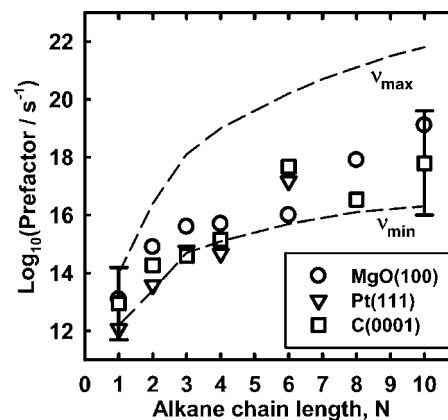


FIG. 7. Preexponential factors vs *n*-alkane chain length for desorption of small *n*-alkanes from Pt(111), C(0001)/Pt(111), and MgO(100). The dashed lines are calculated limits on the prefactor based on the models discussed in Ref. 1 and summarized in the text. These limits are functions of the desorption temperature (which is different for each substrate). For clarity we have only plotted one line each for ν_{min} and ν_{max} , using the desorption temperatures from Pt to compute ν_{min} and the desorption temperatures from MgO to compute ν_{max} , so as to display the tightest limits on prefactors in this plot. Uncertainty in the prefactor values is estimated to be not greater than $\pm 10\%$ in the log of the prefactor. We indicate this by error bars on the data points for methane and *n*-decane on C(0001), but omit the other error bars for clarity of presentation.

adsorbate-substrate interaction potential and is beyond the scope of this work. [Detailed molecular dynamics simulations of small *n*-alkane ($N=1-12$) desorption from Au(111) (Ref. 19) and from C(0001) (Ref. 20) using semiempirical interaction potentials have been reported by Fichthorn and co-workers.] However, we can make some assumption about the degrees of freedom available to the molecules in the adsorbed (initial) state in order to calculate upper and lower limits for q_{ads} , which in turn allows us to determine upper and lower limits for the possible range of prefactors. These limits bound our experimental results, as shown in Fig. 7.

The maximum, physically reasonable prefactor is calculated by considering the lower limit of the adsorbate partition function, q_{ads} , in Eq. (2). In this scenario we consider the adsorbed molecule to be fully hindered in all translational and rotational modes, i.e., we take the partition function to be one. In that case, when the molecule desorbs from the surface into the transition state where it has three free rotational and two free translational modes, its entropy gain (and

TABLE I. Summary of inversion-optimization analysis results for small *n*-alkane desorption from MgO(100), C(0001)/Pt(111), and Pt(111). The log of the desorption prefactor is listed for each molecule and surface as well as the desorption energy at 0.5 ML coverage.

C _N H _{2N+2} N	log ₁₀ [prefactor (s ⁻¹)]			Desorption energy (kJ/mol)		
	MgO(100)	C(0001)	Pt(111)	MgO(100)	C(0001)	Pt(111)
1	13.1	13.0	12.1	12.1	14.1	15.2
2	14.9	14.3	13.6	22.2	24.6	28.9
3	15.6	14.6	14.8	29.0	32.1	41.5
4	15.7	15.2	14.7	34.9	40.8	50.9
6	16.0	17.7	17.2	46.4	63.0	79.8
8	17.9	16.5	...	62.9	72.6	...
10	19.1	17.8	...	77.9	91.4	...

TABLE II. Constants for use in Eqs. (3) and (5) to evaluate ν_{\min} and ν_{\max} for adsorbed *n*-alkanes of chain length *N*. α_{\min} and α_{\max} are constants calculated from the moments of inertia for each of the *n*-alkane molecules (Ref. 1).

C_NH_{2N+2} <i>N</i>	$\nu_{\min} = \alpha_{\min} T^x$		$\nu_{\max} = \alpha_{\max} T^{3.5}$
	<i>x</i>	α_{\min} ($s^{-1} K^{-x}$)	α_{\max} ($s^{-1} K^{-3.5}$)
1	1	2.13×10^{10}	1.40×10^8
2	1.5	1.94×10^{10}	6.88×10^9
3	2	2.31×10^{10}	1.62×10^{11}
4	2	4.07×10^{10}	6.94×10^{11}
5	2	6.10×10^{10}	1.68×10^{12}
6	2	9.62×10^{10}	4.42×10^{12}
7	2	1.24×10^{11}	9.67×10^{12}
8	2	1.64×10^{11}	1.78×10^{13}
9	2	2.20×10^{11}	3.34×10^{13}
10	2	2.40×10^{11}	5.20×10^{13}

thus prefactor) is maximized. The partition function of the molecule in the initial state is minimized and so the ratio in Eq. (2) is maximized. Using Eq. (2) with the partition functions of the molecule¹ we calculate the physical upper limit on the prefactor, ν_{\max} ,

$$\nu_{\max} = \alpha_{\max} T^{3.5}, \quad (3)$$

where α_{\max} is a constant with units $s^{-1} K^{-3.5}$ and is a function of the moments of inertia of the molecule (see Table III in Ref. 1) and of physical constants. Values of α_{\max} for small *n*-alkanes ($N=1-10$) are listed in Table II. The values for the chain length range $N=3-10$ increase in a power law form with chain length, *N*, and are fitted well by the function

$$\alpha_{\max} = 10^{8.91} N^{4.81}. \quad (4)$$

From Eq. (3) we calculate ν_{\max} at the desorption temperature of each of the alkanes from Pt(111) and from C(0001). These values (along with the desorption temperatures) are listed in Table III. Compared to the prefactor values obtained from the inversion-optimization analysis in this study on Pt(111) and C(0001) [Table I and Fig. 7], the values for ν_{\max} are uniformly larger by two to four orders of magnitude and have a stronger chain length dependence. We conclude that this immobile adsorbate model, which gives an upper limit on the prefactor based on physical arguments, overestimates the magnitude and chain length dependence of the prefactor. The calculated value of ν_{\max} for each of the molecules is largest for desorption from Pt(111) and smallest for desorption from MgO(100), due to the difference in desorption temperature. The dashed line in Fig. 7 represents the ν_{\max} values for desorption from MgO(100), which gives the tightest constraint on the data points. The ν_{\max} values for desorption from Pt(111) and C(0001), which are slightly larger than those for MgO(100), are omitted from Fig. 7 for clarity of presentation. [Likewise, only ν_{\min} values for Pt(111) are shown.]

The opposite limit is the minimum, physically reasonable prefactor calculated by considering the case where the adsorbate partition function, q_{ads} is maximized. Here the degrees of freedom of the molecule in the adsorbed state are maximized by assuming a corrugation-free surface potential so that the adsorbate is able to rotate and translate freely in

the plane of the surface and along its axis, but not out of plane. Thus, the entropy gain upon molecule desorption is minimized. In this case, the initial state partition function is large and cancels most of the transition state partition function in Eq. (2). The minimum limit, ν_{\min} , calculated from the partition functions of the molecule,¹ can be expressed as a function of temperature as

$$\nu_{\min} = \alpha_{\min} T^x, \quad (5)$$

where $x=1$ for $N=1$, $x=1.5$ for $N=2$, and $x=2$ for $N=3-10$, and α_{\min} is a constant with units $s^{-1} K^{-x}$. The value x is different for methane and ethane since these have more free rotation modes on the surface due to their simple geometry (ν_{\min} for methane is reduced to calculating $k_B T/h$ at the desorption temperature). Values for the constant α_{\min} are listed in Table II and for $N=3-10$ are fitted well by the function

$$\alpha_{\min} = 10^{9.41} N^{2.00}. \quad (6)$$

We have evaluated ν_{\min} for each desorption temperature listed in Table III. These values have a noticeable chain length dependence but not as strong as the experimental values.

Since these limits depend on the desorption temperature of the molecule, the values will be slightly different for each substrate. For clarity in Fig. 7 we have only plotted the lower limit for Pt(111) and the upper limit for MgO(100), which give the tightest constraint on the data. The best fit values from our experimental results fall within or near (within the error bars of) these limits. It is critical that the rise in prefactor that we observe be accounted for in the TPD analysis or substantial errors in the desorption energies will result, as discussed in Ref. 1. By neglecting the prefactor increase with chain length, the desorption energy scaling with chain length has an unphysically large *y*-intercept value. We note that the prefactors for desorption from MgO(100) are larger than for the other substrates for each of the molecules except *n*-hexane. The MgO prefactors fall, on average, midway between the prefactor limits, whereas the C and Pt prefactors tend to lie close to the minimum prefactor limits. A simple interpretation for this behavior is that since the MgO surface is an ionic surface with both cations and anions in the top-most layer, the surface potential of an adsorbate on that surface is expected to have a higher corrugation than on the close-packed Pt or C surfaces. The molecules adsorbed on MgO may be more constrained in the degrees of freedom available to them, whereas on the Pt and C surfaces, the molecules behave more like a 2D gas (e.g., free rotors). Therefore, the entropy gain during desorption from the MgO substrate is larger than for the other substrates.

D. Desorption energy

Using the best fit prefactors, we calculated the desorption energy versus coverage for each of the molecules studied, which we have plotted in Fig. 8 over the coverage range of 0–0.8 ML on (a) MgO(100), (b) C(0001)/Pt(111), and (c) Pt(111). In Fig. 8 we have plotted an empirical equation whose parameters were fitted to the desorption energy data

TABLE III. Summary of TPD results for n -alkanes of chain length $N=1-10$ on Pt(111) and on C(0001) from this and prior works. The desorption temperature T_{des} is reported from each study as well as the heating ramp rate β . The reported prefactor, ν , and desorption energy, E_{des} , from each study are listed (* indicates an assumed prefactor value rather than one obtained experimentally). We also list the desorption energy E_{des} calculated from the Redhead analysis, Eq. (8), using the reported desorption temperature. The reported desorption temperature and ramp rate of each study were used to calculate maximum and minimum limits on the prefactor based on the models discussed in the text and these were used to calculate limits on the desorption energy using the Redhead equation.

C_NH_{2N+2} N	T_{des} (K)	β (K/s)	Reported		Redhead analysis E_{des} (kJ/mol) $\nu=10^{13} \text{ s}^{-1}$	Minimum limit		Maximum limit		Literature reference
			\log_{10} [$\nu(\text{s}^{-1})$]	E_{des} (kJ/mol)		\log_{10} [ν_{min} (s^{-1})]	E_{min} (kJ/mol)	\log_{10} [ν_{max} (s^{-1})]	E_{max} (kJ/mol)	
Pt(111)										
1	63	0.6	12.1	15.2	16.3	12.1	15.3	14.5	18.0	Present work
	64	2	13.0*	16.1	16.0	12.1	14.9	14.5	17.7	9 and 11
2	106	0.6	13.6	28.9	27.9	13.3	28.6	16.9	35.7	Present work
	115	2	13.0*	36.8	29.2	13.4	30.1	17.1	38.0	9 and 11
3	139	0.6	14.8	41.5	36.9	14.7	41.2	18.7	51.7	Present work
	150	2	13.0*	41.2	38.4	14.7	43.2	18.8	54.7	9 and 11
4	171	0.6	14.7	50.9	45.7	15.1	52.3	19.7	66.9	Present work
	188	4	13.0*	60.2	47.5	15.2	55.2	19.8	71.3	9 and 10
	166	10	11.0	34.3	40.5	15.1	47.0	19.6	60.9	8
5	195	10	11.6	42.7	47.9	15.4	56.5	20.2	74.0	8
6	229	0.6	17.2	79.8	61.7	15.7	73.2	20.9	95.5	Present work
	239	2	13.0*	61.9	62.3	15.7	74.5	21.0	97.9	7
7	256	2	13.0*	66.4	66.8	15.9	80.7	21.4	107	7
8	277	2	13.0*	72.0	72.5	16.1	88.5	21.8	118	7
9	286	2	13.0*	74.2	74.7	16.3	92.0	22.1	123	7
10	297	2	13.0*	...	77.7	16.3	96.1	22.4	129	7
C(0001)										
1	55	0.6	13.0	14.1	14.2	12.1	13.2	14.2	15.5	Present work
2	87	0.6	14.3	24.6	22.8	13.2	23.1	16.6	28.6	Present work
3	110	0.6	14.6	32.1	29.0	14.5	32.0	18.4	40.0	Present work
4	135	0.6	15.2	40.8	35.8	14.9	40.5	19.3	51.7	Present work
5	171	2.0	19.6	65.0	44.0	15.3	51.2	20.0	66.5	15
6	179	0.6	17.7	63.0	47.9	15.5	56.2	20.5	73.0	Present work
	193	2.0	19.6	73.6	49.9	15.6	59.0	20.7	77.4	15
7	213	2.0	19.6	81.5	55.2	15.8	66.1	21.1	87.5	15
8	218	0.6	16.5	72.6	58.6	15.9	70.4	21.4	93.0	Present work
	230	2.0	19.6	88.2	59.7	15.9	72.3	21.5	96.3	15
10	254	0.6	17.8	91.4	68.6	16.2	83.7	22.1	112	Present work
	263	2.0	19.6	101	68.6	16.2	84.4	22.2	114	15

as described below. In Fig. 8(c), place-holder dashed lines are drawn for estimates of the desorption energies of n -octane and n -decane from Pt(111), which were not accessible in our experiments, as discussed above. These estimates were made by linear extrapolation of the desorption energies

at 0.5 ML coverage of the smaller n -alkanes from Pt(111). We note that the general line shape of the desorption energy data is reproduced well by this energy curve and is similar for each molecule and that the energy increases monotonically with n -alkane chain length. In each case the energy

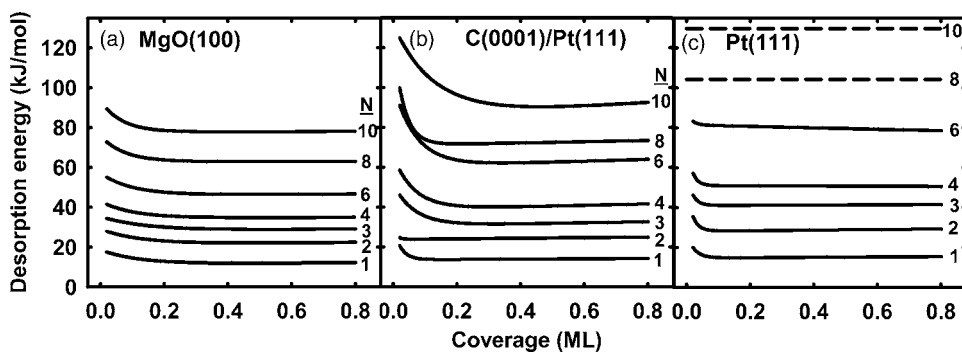


FIG. 8. Desorption energy vs n -alkane coverage for seven n -alkanes desorbing from (a) MgO(100), (b) C(0001)/Pt(111), and (c) Pt(111). In the case of desorption from Pt(111), dissociation of the n -octane and n -decane molecules on the substrate prevented a full analysis of those data. The place-holder dashed lines in (c) are drawn at estimated values of the desorption energy of those molecules at 0.5 ML coverage, based on a linear extrapolation of the desorption energies of the smaller n -alkanes from Pt(111).

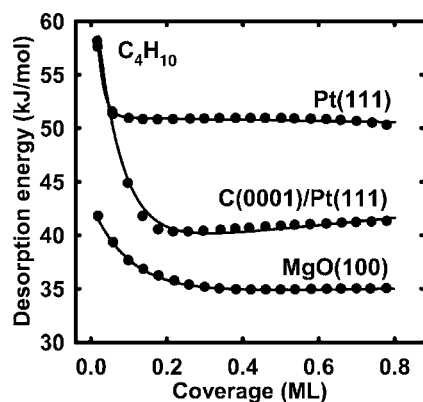


FIG. 9. Desorption energy vs coverage for *n*-butane desorption from MgO(100), C(0001)/Pt(111), and Pt(111). The solid points are desorption energy values calculated from an experimental TPD spectrum using the “best fit prefactor” in the inversion method described in the text. The solid lines are fits to these points using Eq. (7). The resulting fit parameters are listed in Table IV.

decreases steeply with increasing coverage in the range of approximately 0–0.2 ML. This corresponds to the coverage range where desorbing molecules are affected by substrate defect sites (e.g., step edges). The energy in this range represents a convolution of the desorption energy on the terrace and the desorption energies of the various species of defect sites. Above ~ 0.3 ML the desorption energy is nearly constant with coverage as the molecules are desorbing from the terrace sites. However, there is a very small positive slope in most of the curves, due to attractive interactions between the adsorbate molecules. In two energy versus coverage curves [$N=4$ and 6 on Pt(111), Fig. 8(c)] there is a slight negative slope, corresponding to monolayer peak shift to lower temperature with increasing coverage, as discussed above.

Each energy curve was fitted to the analytic form

$$E_d(\theta) = E_0 + \gamma\theta + E_{\text{def}}e^{-\theta/\theta_{\text{def}}}. \quad (7)$$

The quality of the fit of this equation to the desorption energy data is illustrated in Fig. 9 for the *n*-butane desorption

energy on each of the three substrates (points are desorption energy data, whereas lines are empirical fits). The fitting parameters are listed in Table IV. For each molecule this function fits the desorption energy well as in Fig. 9. The physical significance of the fit parameters has been discussed in Ref. 1. The first term E_0 represents the desorption energy one would obtain by extrapolating the linear region of the coverage-dependent energy curve back to the limit of zero coverage. This is the number that could most readily be interpreted as the activation energy for desorption of an isolated adsorbate from a terrace site (i.e., in the absence of defect sites and adsorbate-adsorbate interactions). The factor γ in the second term of Eq. (7) is the increase in desorption energy per monolayer increase in coverage due to lateral interactions between adsorbates. The factor E_{def} in the third term of Eq. (7) is the energy difference between E_0 and the measured desorption energy at zero coverage, $E_d(0)$, and is related to the difference between the adsorption energy of an *n*-alkane molecule adsorbed on a terrace site compared to one adsorbed at a defect site. It may be more instructive to consider the behavior of the ratio $(E_0 + E_{\text{def}})/E_0$ (listed in Table IV), which compares the adsorption energy of a molecule at a defect site ($E_0 + E_{\text{def}}$) to that of a molecule at a terrace site (E_0). The factor θ_{def} corresponds to the rate at which the influence of defect sites on the energy decays with increasing coverage. It is related to the density (fractional area) of defect sites on the surface as well as to the degree to which defect sites influence the adsorption of molecules that are near molecules adsorbed at defects. We note that the parameter θ_{def} is significantly larger for propane, *n*-butane, and *n*-hexane on C(0001)/Pt(111) than for the same molecules on Pt(111). This is most likely due to a greater number of grain boundaries and other defect structures on the graphite film compared to the clean single crystal metal surface. In each case, the increase in energy with decreasing coverage in the low coverage limit (<0.2 ML) seems to be much sharper on the Pt surface than on MgO or C/Pt. These observations are consistent with the Pt crystal being the highest quality (i.e., low defect density) of the three substrates; an expected

TABLE IV. Parameter values for the best fit of the analytic function Eq. (7), to the experimentally obtained coverage-dependent desorption energies for each *n*-alkane studied on Pt(111) and C(0001)/Pt(111).

<i>n</i> -alkane (C_NH_{2N+2})	E_0 (kJ/mol)	γ (kJ/mol ML)	E_{def} (kJ/mol)	θ_{def} (ML)	$(E_0 + E_{\text{def}}/E_0)$
Pt(111)					
Methane ($N=1$)	14.8	0.880	12.7	0.023 1	1.86
Ethane ($N=2$)	28.2	1.23	22.1	0.018 3	1.78
Propane ($N=3$)	41.1	0.557	17.2	0.017 0	1.42
<i>n</i> -butane ($N=4$)	51.0	−0.536	22.0	0.016 3	1.43
<i>n</i> -hexane ($N=6$)	81.4	−3.59	5.77	0.018 1	1.07
C(0001)/Pt(111)					
Methane ($N=1$)	13.6	0.931	16.8	0.023 9	2.24
Ethane ($N=2$)	23.8	1.39	6.46	0.009 98	1.27
Propane ($N=3$)	30.6	2.61	20.8	0.067 3	1.68
<i>n</i> -butane ($N=4$)	38.9	3.42	27.0	0.064 8	1.69
<i>n</i> -hexane ($N=6$)	60.3	4.67	40.9	0.071 4	1.68
<i>n</i> -octane ($N=8$)	71.0	3.02	52.9	0.033 8	1.75
<i>n</i> -decane ($N=10$)	84.5	10.0	47.1	0.129	1.56

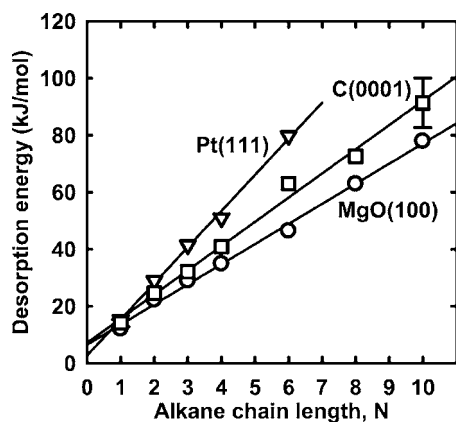


FIG. 10. Desorption energy vs n -alkane chain length for desorption of small n -alkanes from Pt(111), C(0001)/Pt(111), and MgO(100) (triangles, squares, and circles, respectively). The desorption energies plotted here are taken from the curves in Fig. 8 at 0.5 ML coverage. The solid lines are linear fits to each data set (fit parameters given in Table V) and demonstrate the linear increase in energy with n -alkane chain length and a y -intercept value small compared to the slope of the line.

observation as the Pt surface is the only of the three which is a bulk single crystal sample. In Fig. 9, the desorption energy of n -butane on the C(0001)/Pt(111) surface turns up sharply in the low-temperature limit and at the lowest coverage data point matches the desorption energy value for Pt(111). This may be due to small “cracks” in the graphite layer or small regions of bare Pt where the n -butane can adsorb.

We note that the desorption energy increases in the order MgO(100) < C(0001)/Pt(111) < Pt(111) for each of the

n -alkanes studied. The larger desorption energies on Pt(111) are at least partially attributable to the higher polarizability of Pt, which would lead to a stronger instantaneous induced dipole–induced dipole (van der Waals) interaction. It is probably also due to the large work function of Pt [6.10 eV (Ref. 33)], and its associated electric field near the surface, which induces a substantial permanent dipole moment in adsorbed alkanes.²⁹ There may also be some agostic bonding of the n -alkanes on Pt (i.e., three-center covalent bonding involving the interaction of Pt with a C–H bond), which is thought to play an important role for cyclohexane and other alkanes on Pt(111).³⁴

We summarize the desorption energy at 0.5 ML coverage for each molecule versus chain length in Table I and in Fig. 10 for desorption from MgO(100), C(0001)/Pt(111), and Pt(111). The solid lines in Fig. 10 are linear fits to the desorption energies. The desorption energy increases nearly linearly with n -alkane chain length on each substrate. The slopes and y -intercept values of these lines are listed in Table V.

IV. REEVALUATION OF PREVIOUS STUDIES OF n -ALKANE DESORPTION

There have been several interesting studies of n -alkane desorption kinetics versus chain length on Pt(111) and C(0001) which we will review and compare to our results. In Table III we summarize the results of three groups along with our own results for n -alkane desorption from these substrates in order to make a direct comparison over the range of

TABLE V. Linear best fit parameters to experimental desorption energy vs n -alkane chain length in Fig. 13, $E_d = E_0 + \Delta E N$. Fit parameters are listed for fits to the reported E_{des} in each work as well as to the E_{min} and E_{max} values, which we calculated based on the prefactor limit models discussed in the text and the reported desorption temperatures in each work.

Reference		y -intercept, E_0 (kJ/mol)	Slope, ΔE (kJ/mol C segment)	Ratio, $E_0/\Delta E$ (C segment)
Pt(111)				
Madix and co-workers	Reported E_{des}	4.40	13.7	0.321
	E_{min}	1.92	13.7	0.140
	E_{max}	0.470	18.1	0.0260
Bishop <i>et al.</i>	Reported E_{des}	39.5	3.86	10.2
	E_{min}	42.8	5.45	7.85
	E_{max}	51.3	7.99	6.42
Salmeron and Somorjai	Reported E_{des}	0.700	8.40	0.0833
	E_{min}	9.00	9.50	0.947
	E_{max}	8.50	13.1	0.649
Present work	Reported E_{des}	2.67	12.7	0.210
	E_{min}	5.24	11.5	0.456
	E_{max}	4.23	15.4	0.275
C(0001)				
Paserba and Gellman	Reported E_{des}	30.5	7.13	4.28
	E_{min}	19.2	6.59	2.91
	E_{max}	20.7	9.39	2.20
Present work	Reported E_{des}	7.11	8.50	0.836
	E_{min}	7.77	7.78	1.00
	E_{max}	7.32	10.7	0.684

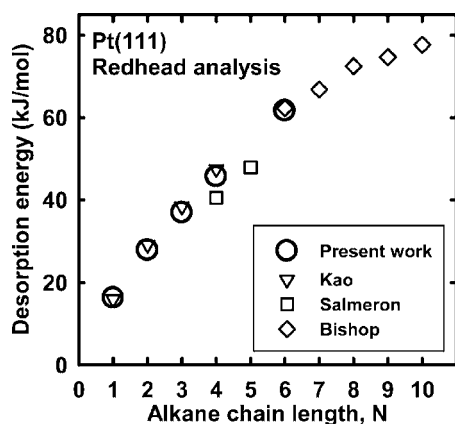


FIG. 11. Comparison of *n*-alkane desorption energies from Pt(111) vs *n*-alkane chain length from four independent studies. The reported desorption temperature and heating ramp rate were used with the Redhead equation [Eq. (3)], assuming prefactor of 10^{13} s^{-1} to compute the desorption energies shown here (Table III). This common analysis approach was chosen to compare the experimental results of the studies. Studies for $N=1-4$ by the Madix and co-workers (Refs. 9–11), $N=4-5$ by Salmeron and Somorjai (Ref. 8), and $N=6-10$ by Bishop *et al.* (Ref. 7).

n-alkane molecules that we have studied. Monolayer desorption peak temperature and heating ramp rate are given for each experiment. The first-order Polanyi-Wigner equation is evaluated at the desorption peak temperature, T_{des} , and rearranged in the form of the Redhead equation,^{35–37}

$$\ln\left(\frac{\beta}{T_{\text{des}}^2}\right) = -\ln\left(\frac{E_d}{k_B\nu}\right) - \frac{E_d}{k_B T_{\text{des}}}, \quad (8)$$

where β is the heating rate and k_B is the Boltzmann constant. Using this equation with the peak temperatures and heating rates in Table III we can make a direct comparison between the desorption experiments of the three prior groups and our own work. In order to make an equal comparison between the different studies, we evaluate Eq. (8) to find the desorption energy for each molecule, assuming the traditional prefactor value of $\nu=10^{13} \text{ s}^{-1}$, and using the appropriate values of peak temperature and heating rate (Table III). The resulting energies for experiments on Pt(111) are listed in the sixth column of Table III and are plotted versus *n*-alkane chain length in Fig. 11. We see that the agreement between the results of these studies is very good and nearly falls on a common curve. It is instructive to note here that since we have chosen the common prefactor of 10^{13} s^{-1} for the entire molecule range rather than varying the prefactor with *n*-alkane chain length, the desorption energy points do not fall on a straight line. This is in contrast to Fig. 10 where the desorption prefactors used to calculate the desorption energies were allowed to increase with chain length and so the desorption energy versus chain length points are fitted well by a linear function. We also note that in Fig. 11 the data of Bishop *et al.* have a noticeably smaller slope (incremental increase in desorption energy per unit increase in chain length) compared to the other three studies. Their data are for the longer *n*-alkane molecules, which we were not able to study due to the dissociation of these molecules on the Pt(111) surface. Unfortunately, there is insufficient detail in their paper to determine the cleanliness of their surface, but

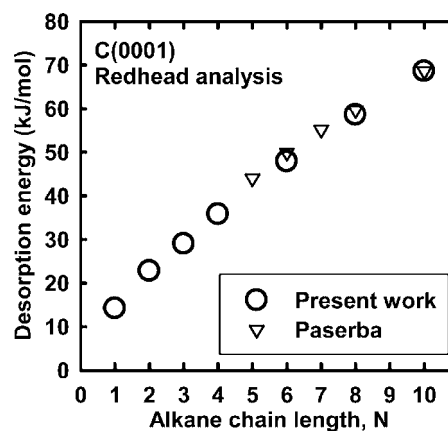


FIG. 12. Comparison of *n*-alkane desorption energies vs *n*-alkane chain length on C(0001). We compare our results (circles) to those of Paserba and Gellman (triangles) (Ref. 15). The reported desorption temperature and heating ramp rate were used with the Redhead equation [Eq. (3)], assuming prefactor of 10^{13} s^{-1} to compute the desorption energies shown here (Table III). This common analysis approach was chosen to compare the experimental results of the studies.

we suspect that their results may have also been affected by dissociation of the longer *n*-alkanes (e.g., *n*-octane and *n*-decane). In that case the desorption of the longer molecules from a (partially) graphitized surface would yield a lower desorption energy and could lead to the observed effect of the desorption energy having a smaller than expected slope.

The lower section of Table III lists the results of our desorption experiments on graphite as well as those of Paserba and Gellman¹⁵ for $N=1-10$. The sixth column of the table lists the desorption energies evaluated for a prefactor of 10^{13} s^{-1} and these values are plotted versus chain length in Fig. 12. Again, the agreement between these two studies is very good. We see in this figure, as we did in Fig. 11, that by assuming a constant prefactor in this analysis there is some curvature to the data (negative second derivative). It is essential that the prefactor be allowed to vary in the data analysis in order to get a good representation of the desorption kinetics of the small *n*-alkanes.

We show the importance of allowing for the prefactor increase by using the prefactor limits, ν_{min} and ν_{max} , to calculate limits on the desorption energy using the Redhead equation. The desorption temperatures from each of the studies are used in Eqs. (3) and (5) to calculate ν_{max} and ν_{min} respectively. These limits are listed in Table III and are used in Eq. (8) to calculate E_{max} and E_{min} , also listed in Table III, which represent limits on the desorption energy values. We have already pointed out that several previous studies of desorption energy versus *n*-alkane chain length have fitted well to a linear function but with a large *y*-intercept value, which cannot be justified physically. In Fig. 13, we plot the results of several studies, including the present one, for *n*-alkane desorption from Pt(111) and C(0001) as solid circles with linear fits (solid lines). We also plot the values of E_{min} and E_{max} that we have calculated according to the published desorption temperatures (Table III) from the studies and the corresponding values of ν_{min} and ν_{max} . These data are fitted to straight lines (dashed lines in Fig. 13) and the slope and

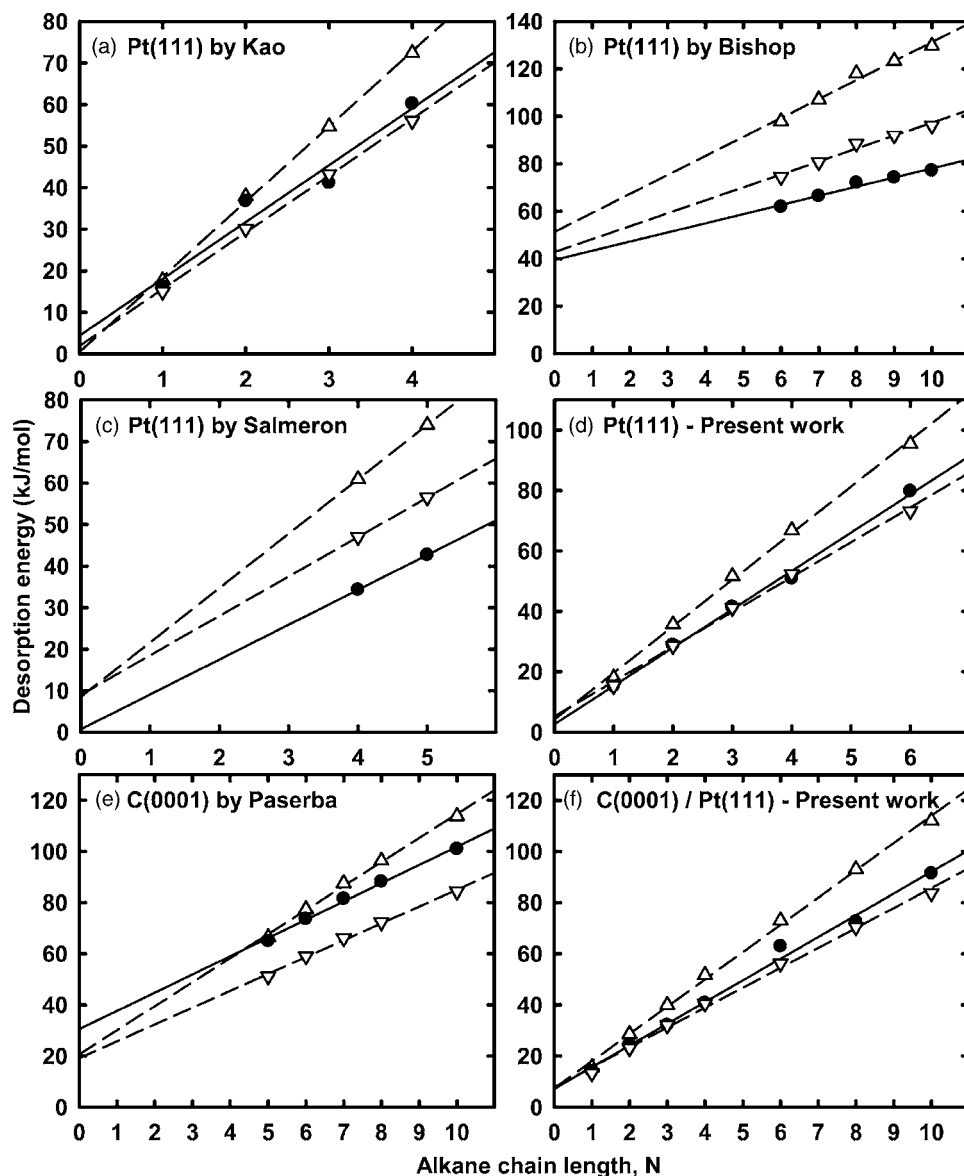


FIG. 13. Comparison of desorption energies vs chain length from the present work and four other studies on Pt(111) and C(0001). The desorption energies from the present work are from the inversion-optimization analysis discussed in the text [solid circles in (d) and (f)]. In frames (a)–(c) and (e), the solid points represent the desorption energies reported in those works. The solid lines are fits to these solid points. Using the reported desorption temperatures in each study, the upper and lower limits on the desorption prefactor were calculated from Eqs. (3) and (5). These were used in the Redhead equation to calculate the limits on the desorption energy which are plotted as hollow triangles here (upward pointing triangles for E_{\max} and downward pointing triangles for E_{\min}). The dashed lines are linear fits to these points. The results of the linear fits are given in Table V.

y -intercept values for each of these fit lines are listed in Table V. We find that in two of these previous studies [Figs. 13(b) and 13(e)] there is a marked decrease in the ratio of the y -intercept to the slope. However, in the case of the data from the paper of Bishop *et al.* [Fig. 13(b)] there is still a significant y -intercept value. As we noted in the discussion of Fig. 11 above, there is some discrepancy in the data of Bishop

et al. compared to other studies on Pt (noticeably different slope in energy versus chain length plot), which also leads to this large y -intercept. In the case of the work of Paserba and Gellman, we noted in the Introduction that they assumed a constant prefactor over this range of molecules but that this assumption was based on experiments over a wide range of molecules up to $N=60$. Their use of a constant prefactor in the size range considered here ($N=5-10$) leads to a less than linear increase in the desorption energy with chain length, as noted above with regard to Fig. 12, and results in a large y -intercept value when the data are fitted to a line [Table V and Fig. 13(e)]. We note that we see the same effect in our data when analyzed using a constant prefactor (Fig. 12), and

find that if we fit the points (based on $\nu=10^{13} \text{ s}^{-1}$ in analysis) in the range $N=6-10$ to a linear function we also obtain a large y -intercept value ($E_0=17.0 \text{ kJ/mol}$, $\Delta E=5.18 \text{ kJ/mol C segment}$, and $E_0/\Delta E=3.28 \text{ C segment}$).

In the studies in Figs. 13(a), 13(c), 13(d), and 13(f), which already had low y -intercept/slope ratios, the decrease in the ratio with the prefactor limits is less dramatic. As discussed in the Introduction, one would expect based on pairwise van der Waals interactions that there should be a positive y -intercept in such plots, but that its magnitude should be small compared to the slope. The decrease in the y -intercept/slope ratios that results from the more rigorous analysis of TPD data presented here thus can be considered as a significant improvement, which clarifies significantly our understanding of the interactions of n -alkanes with solid surfaces. Thus, the earlier experimental studies^{3,7,15,17} which raised concerns about the implications of the large y -intercepts can now be understood more satisfactorily. As our results show, this is primarily related to allowing for an increasing desorption prefactor with alkane chain length. This result is also consistent with the molecular dynamics

simulations of Fichthorn and co-workers. As we noted earlier, they predicted a significant increase in prefactor with chain length for alkane desorption from the C(0001) surface²⁰ and the Au(111) surface.¹⁹ Their results are in very good qualitative agreement with our experimental data from three substrates and, in the case of C(0001), also in excellent quantitative agreement.

V. CONCLUSIONS

We have studied the desorption kinetics of small *n*-alkane molecules (C_NH_{2N+2}) from Pt(111) and C(0001)/Pt(111). We find that on these surfaces the desorption energy of the *n*-alkanes increases linearly with chain length over the range of molecules studied ($N=1-10$). We also find that the kinetic prefactor for desorption increases with chain length by several orders of magnitude. This supports our hypothesis that the similar result of a large prefactor increase with chain length for small *n*-alkane desorption from MgO(100) (Ref. 1) was not particular to the MgO(100) surface, but is a general result for small *n*-alkane desorption from any substrate. From simple statistical mechanical arguments, it has been demonstrated here briefly and in more detail elsewhere¹ that the prefactor should show an increase of several orders of magnitude due to the increase in the rotational and translation entropy gains of the *n*-alkane molecules upon desorption. This can be used as a general rule of thumb for *n*-alkane desorption from any surface, as has been confirmed here for two different surfaces, a metal Pt(111) surface and a graphitic C(0001) surface. Thus, a strong (several orders of magnitude) increase in the desorption prefactor of the small *n*-alkanes ($N=1-10$) with chain length should be expected for desorption from any substrate. Prior studies of *n*-alkane desorption from metal surfaces had found an unphysically large γ -intercept in the desorption energy versus chain length dependence. We have shown that by considering the prefactor increase with chain length in a reanalysis of their results, we can resolve this γ -intercept issue to some degree in these other studies.

ACKNOWLEDGMENTS

Two of the authors (B.D.K. and Z.D.) were funded by the U.S. Department of Energy Office of Basic Energy Sciences (OBES) Chemical Sciences and Materials Sciences Divisions. One of the authors (C.T.C.) acknowledges support by the OBES Chemical Sciences Division. Another author (S.L.T.) was supported by a graduate student fellowship award from the University of Washington/Pacific Northwest National Laboratory (PNNL) Joint Institute for Nanoscience. All of the experimental work was performed in the Environmental Molecular Sciences Laboratory, a national scientific

user facility sponsored by the Department of Energy's Office of Biological and Environmental Research and located at PNNL. PNNL is a multiprogram National Laboratory operated for the U.S. Department of Energy by Battelle Memorial Institute under Contract No. DE-AC06-76RLO 1830.

- ¹S. L. Tait, Z. Dohnalek, C. T. Campbell, and B. D. Kay, *J. Chem. Phys.* **122**, 164708 (2005).
- ²J. Pawela-Crew and R. J. Madix, *Surf. Sci.* **339**, 8 (1995).
- ³S. M. Wetterer, D. J. Lavrich, T. Cummings, S. L. Bernasek, and G. Scoles, *J. Phys. Chem. B* **102**, 9266 (1998).
- ⁴R. Z. Lei, A. J. Gellman, and B. E. Koel, *Surf. Sci.* **554**, 125 (2004).
- ⁵B. A. Sexton and A. E. Hughes, *Surf. Sci.* **140**, 227 (1984).
- ⁶A. V. Tepyakov, A. B. Gurevich, M. X. Yang, B. E. Bent, and J. G. G. Chen, *Surf. Sci.* **396**, 340 (1998).
- ⁷A. R. Bishop, G. S. Girolami, and R. G. Nuzzo, *J. Phys. Chem. B* **104**, 754 (2000).
- ⁸M. Salmeron and G. A. Somorjai, *J. Phys. Chem.* **85**, 3835 (1981).
- ⁹J. F. Weaver, A. F. Carlsson, and R. J. Madix, *Surf. Sci. Rep.* **50**, 107 (2003).
- ¹⁰J. F. Weaver, M. Ikai, A. Carlsson, and R. J. Madix, *Surf. Sci.* **470**, 226 (2001).
- ¹¹C. L. Kao and R. J. Madix, *J. Phys. Chem. B* **106**, 8248 (2002).
- ¹²C. L. Kao and R. J. Madix, *Surf. Sci.* **557**, 215 (2004).
- ¹³J. L. Brand, M. V. Arena, A. A. Deckert, and S. M. George, *J. Chem. Phys.* **92**, 5136 (1990).
- ¹⁴R. M. Slayton, C. M. Aubuchon, T. L. Camis, A. R. Noble, and N. J. Tro, *J. Phys. Chem.* **99**, 2151 (1995).
- ¹⁵K. R. Paserba and A. J. Gellman, *J. Chem. Phys.* **115**, 6737 (2001).
- ¹⁶A. J. Gellman and K. R. Paserba, *J. Phys. Chem. B* **106**, 13231 (2002).
- ¹⁷K. R. Paserba and A. J. Gellman, *Phys. Rev. Lett.* **86**, 4338 (2001).
- ¹⁸J. K. Simons, S. P. Frigo, J. W. Taylor, and R. A. Rosenberg, *Surf. Sci.* **346**, 21 (1996).
- ¹⁹K. A. Fichthorn and R. A. Miron, *Phys. Rev. Lett.* **89**, 196103 (2002).
- ²⁰K. E. Becker and K. A. Fichthorn, *J. Chem. Phys.* **125**, 184706 (2006).
- ²¹S. L. Tait, Z. Dohnalek, C. T. Campbell, and B. D. Kay, *J. Chem. Phys.* **122**, 164707 (2005).
- ²²Z. Dohnalek, G. A. Kimmel, S. A. Joyce, P. Ayotte, R. S. Smith, and B. D. Kay, *J. Phys. Chem. B* **105**, 3747 (2001).
- ²³Z.-P. Hu, D. F. Ogletree, M. A. Van Hove, and G. A. Somorjai, *Surf. Sci.* **180**, 433 (1987).
- ²⁴N. R. Gall, E. V. Rutkov, and A. Y. Tontegode, *Int. J. Mod. Phys. B* **11**, 1865 (1997).
- ²⁵A. Y. Tontegode, *Prog. Surf. Sci.* **38**, 201 (1991).
- ²⁶J. J. Vajo, Y.-K. Sun, and W. H. Weinberg, *Appl. Surf. Sci.* **29**, 165 (1987).
- ²⁷J. L. Daschbach, B. M. Peden, R. S. Smith, and B. D. Kay, *J. Chem. Phys.* **120**, 1516 (2004).
- ²⁸J. S. Raut, D. S. Sholl, and K. A. Fichthorn, *Surf. Sci.* **389**, 88 (1997).
- ²⁹K. H. Ernst and C. T. Campbell, *Surf. Sci.* **259**, L736 (1991).
- ³⁰G. A. Kimmel, M. Persson, Z. Dohnalek, and B. D. Kay, *J. Chem. Phys.* **119**, 6776 (2003).
- ³¹J. M. Gay, J. Suzanne, and R. Wang, *J. Phys. (France) Lett.* **46**, L425 (1985).
- ³²D. A. McQuarrie, *Statistical Mechanics* (Harper & Row, New York, 1975).
- ³³G. N. Derry and Z. Ji-Zhong, *Phys. Rev. B* **39**, 1940 (1989).
- ³⁴M. A. Chesters and P. Gardner, *Spectrochim. Acta, Part A* **46**, 1011 (1990).
- ³⁵J. L. Falconer and R. J. Madix, *Surf. Sci.* **48**, 393 (1975).
- ³⁶D. A. King, *Surf. Sci.* **47**, 384 (1975).
- ³⁷P. A. Redhead, *Vacuum* **12**, 203 (1962).